The Astrophysical Journal, 891:57 (14pp), 2020 March 1 https://doi.org/10.3847/1538-4357/ab7339

Calibration of the Tip of the Red Giant Branch

Wendy L. Freedman[1], Barry F. Madore[1,2], Taylor Hoyt[1], In Sung Jang[3], Rachael Beaton[4], Myung Gyoon Lee[5], Andrew Monson[6], Jill Neeley[7], and Jeffrey Rich[2]
[1] Dept. of Astronomy & Astrophysics, Univ. Chicago, 5640 S. Ellis Ave., Chicago, IL 60637, USA; wfreedman@uchicago.edu
[2] The Observatories, Carnegie Institution for Science, 813 Santa Barbara St., Pasadena, CA 91101, USA
[3] Leibniz-Institut für Astrophysik Potsdam (AIP), An der Sternwarte 16, D-14482 Potsdam, Germany
[4] Dept. of Astrophysical Sciences, Princeton University, 4 Ivy Lane, Princeton, NJ 08544, USA
[5] Dept. of Physics & Astronomy, Seoul National University, Gwanak-gu, Seoul 151-742, Republic of Korea
[6] Dept. of Astronomy & Astrophysics, Penn State, 525 Davey Lab, University Park, PA 16802, USA
[7] Dept. of Physics, Florida Atlantic University, 777 Glades Rd., Boca Raton, FL 33431, USA
Received 2019 December 18; revised 2020 February 1; accepted 2020 February 4; published 2020 March 4

Abstract

The tip of the red giant branch (TRGB) method provides one of the most accurate and precise means of measuring the distances to nearby galaxies. Here we present a multi-wavelength, *VIJHK* absolute calibration of the TRGB based on observations of TRGB stars in the Large Magellanic Cloud (LMC), grounded on a geometric distance, determined by detached eclipsing binaries (DEBs). This paper presents a more detailed description of the method first presented by Freedman et al. for measuring corrections for the total line-of-sight extinction and reddening to the LMC. In this method, we use a differential comparison of the red giant population in the LMC, first with red giants in the Local Group galaxy IC 1613, and then with those in the Small Magellanic Cloud (SMC). As a consistency check, we derive an independent calibration of the TRGB sequence using the SMC alone, invoking its geometric distance also calibrated by DEBs. An additional consistency check comes from near-infrared observations of Galactic globular clusters covering a wide range of metallicities. In all cases we find excellent agreement in the zero-point calibration. We then examine the recent claims by Yuan et al., demonstrating that, in the case of the SMC, they corrected for extinction alone while neglecting the essential correction for reddening. In the case of IC 1613, we show that their analysis contains an incorrect treatment of (over-correction for) metallicity. Using our revised (and direct) measurement of the LMC TRGB extinction, we find a value of $H_0 = 69.6 \pm 0.8$ ($\pm 1.1\%$ stat) $\pm$ 1.7 ($\pm 2.4\%$ sys) km s^{-1} Mpc^{-1}.

Unified Astronomy Thesaurus concepts: Observational cosmology (1146); Galaxy distances (590); Interstellar extinction (841); Hubble constant (758)

1. Introduction

The tip of the red giant branch (TRGB) sequence marks the well-understood, abrupt evolutionary transition of low-mass RGB stars onto the lower-luminosity horizontal branch. These RGB stars are powered by a hydrogen-burning shell surrounding an isothermal helium core which is supported by electron degeneracy. Their transition away from the TRGB is initiated by a brief helium flash, a period of thermal runaway whereupon the degeneracy of the core is lifted, and the triple-alpha (helium-burning) process can proceed at a lower luminosity in a gas-pressure-supported core. At this transition, the tip stars rapidly fade in luminosity, settling onto the horizontal branch, burning helium in their core and hydrogen in a surrounding shell. The basic underlying physical explanation for a universal upper limit to the luminosity of an RGB star is theoretically well understood (e.g., Salaris & Cassisi 1997, Bildsten et al. 2012; Serenelli et al. 2017) and, empirically, this distinctive feature in the observed RGB luminosity function is well-known to be an excellent means of measuring the distances in the halos of nearby resolved galaxies: in the *I* band the TRGB is a "standard candle" (e.g., Lee et al. 1993; Rizzi et al. 2007; Serenelli et al. 2017).

Over the past 30 years the TRGB sequence has been measured and successfully used by many independent groups to determine high-precision distances to large numbers of nearby galaxies (e.g., Sakai et al. 2004; Makarov et al. 2006; Rizzi et al. 2007; Dalcanton et al. 2009, 2012; Jang & Lee 2017a, 2017b; McQuinn et al. 2019; Freedman et al. 2019, and references therein). The unique imaging capabilities of the *Hubble Space Telescope* (*HST*), combined with the ease with which the *I*-band tip in particular (see below) can be measured and used to determine distances, have made this method readily accessible and widely applied by the general astronomical community. Indeed, a recent search of the literature (NED 2019 August) shows that there are currently some 900 applications of the TRGB method published for over 300 individual galaxies. A program aimed at optimally determining TRGB distances simply requires targeted observations of the halos of any nearby galaxy, made to sufficient depth to resolve and measure the brightest old Population II red giant stars, which are known to inhabit all stellar halos. Although the method itself is not new, it is only recently that the TRGB method has been applied directly to the determination of H_o (Karachentseva et al. 2003; Mould & Sakai 2008, 2009; Jang & Lee 2017b; Freedman et al. 2019).

One of the distinct advantages of the TRGB method is the fact that the TRGB stars populate the halos of the host galaxy (in contrast to the Cepheids, for example, which are found only in the higher-surface-brightness disk regions). Additionally, the halos of undisturbed galaxies are demonstrably lacking in gas

and devoid of dust, reddening, and extinction. While this latter advantage holds true in the *application* of the TRGB method, the situation is somewhat more complicated when it comes to *calibrating* the TRGB. We consider this aspect of the TRGB calibration in what follows.

It is anticipated that the zero-point calibration of the TRGB will clearly be strengthened when absolute trigonometric parallaxes from *Gaia* become available for significant samples of nearby TRGB stars in the halo of the Milky Way. A preliminary calibration based on the *Gaia* Data Release 2 (DR2) has been published by Mould et al. (2019), which is in broad agreement with earlier calibrations. However, the early-release parallax measurements are still preliminary, and they are subject to known systematic uncertainties (as discussed in Arenou et al. 2018). Anticipating the upcoming DR3 results from *Gaia*, which are still some years away from publication, we have, in the meantime, chosen to use the Large Magellanic Cloud (LMC) to set the absolute calibration for the TRGB. We have then compared this TRGB zero-point with additional, parallel calibrations, each grounded in geometric distances (as is the LMC) derived from the analysis of detached eclipsing binaries (DEBs) in the Small Magellanic Cloud (SMC) (Graczyk et al. 2014) and 47 Tucanae (Thompson et al. 2020). We have used the da Costa & Armandroff (1990; hereafter DCA90) study of RGB stars in Galactic globular clusters, extending the analysis into the near-infrared using 2MASS data and using the new geometric distance to 47 Tucanae based on DEBs for the zero-point calibration.

For well-separated (detached) double-line spectroscopic, binary star systems, the stellar radii can be measured from their photometric and radial-velocity curves. As articulated by Paczyński (1997), the distance to the DEB can then be determined through an empirical calibration of the surface brightness (angular diameter) and color (temperature). The DEB method has been recently and extensively developed by Pietrzyński and collaborators (see Pietrzyński et al. 2019 and references therein) concentrating on late-type giants. These authors find an extremely tight relation between the optical/near-infrared $(V-K)$ color and surface brightness, with an rms scatter of only 0.018 mag, from which they have determined a 1% distance to the LMC.

Using the *HST* Advanced Camera for Surveys (*HST*/ACS), Freedman et al. (2019) applied a calibration of the TRGB, which was subsequently applied to galaxies hosting Type Ia supernovae (SNe Ia), and used to determine a new value of the Hubble constant, anchored to the DEB distance to the LMC. In that work, we briefly described a new method for measuring the extinction for TRGB stars in the LMC, and we provided a preliminary calibration at *VIJHK* wavelengths for the TRGB. Here we provide a more detailed description and update of the method, which makes use of a consistent set of TRGB stars with multi-wavelength data. A clear advantage of this method is that it provides a direct measurement of the extinction, derived from, and applicable to, the TRGB stars themselves.

We begin by illustrating the expected behavior of the TRGB, based on published isochrones spanning a range in metallicity, color, and age. Based on *VI* and *JHK* photometry for TRGB stars in the LMC we then detail our method for measuring the extinction and reddening, and determine a calibration of the TRGB zero-point. We discuss our measurement of the LMC extinction in the context of other recent studies, provide two external consistency checks on our calibration, and present a value for H_0 based on our adopted calibration.

In the Appendix, we address some serious issues arising in the recent paper by Yuan et al. (2019; hereafter Y19). We demonstrate that the adoption of incorrect assumptions has led to an erroneous result, specifically their underestimate of the line-of-sight extinction to the TRGB stars in the LMC.

2. TRGB Theoretical Isochrones

To provide some overall context for the method that we have developed, we first show the *expected behavior* of the TRGB as a function of metallicity, age, and bandpass. For illustrative purposes, we use the PARSEC (Padova and Trieste Stellar Evolutionary Code: http://stev.oapd.inaf.it/cgi-bin/cmd) isochrones (CMD Version 3.3; Bressan et al. 2012; Marigo et al. 2017). We are not aiming here to provide a comprehensive discussion of different TRGB models, but simply to convey, in broad outline, the general behavior of the TRGB as a function of wavelength, age, and metallicity. We note that here and throughout this paper, all magnitudes are on the Vega system.

In Figure 1 (upper panel), we examine the behavior with wavelength of RGB stars with a *range of metallicities* at *V*-, *I*-, and *K*-band wavelengths. Shown are giant branch isochrones with a large range of metallicities spanning $-2.0 < [\mathrm{M/H}] < -0.1$ dex. As is well known, with increasing metallicity the *V*-band isochrones become fainter with wavelength, the *I*-band isochrones have a nearly constant magnitude, and the near-infrared isochrones become brighter.

In Figure 1 (lower panel) we also examine the behavior with wavelength of RGB stars with a *range of ages*. Shown are giant branch isochrones at *V*-, *I*-, and *K*-band wavelengths, with an age spread covering 4×10^9–10^{10} yr, at a fixed metallicity of $[\mathrm{M/H}] = -1.8$ dex. This plot illustrates the overall insensitivity of the giant branch luminosity, at a given wavelength, to the age of older RGB stars. Most of the color width of a composite old (>4 Gyr) stellar population results from a spread in metallicity, not a spread in age. At fixed metallicity an age spread of 4×10^9–10^{10} yr introduces an effective (color-correlated) magnitude scatter of ±0.040 (at *V*), 0.005 (*I*), 0.012 (*J*), 0.023 (*H*), and 0.026 (*K*) mag, respectively. In Figure 2 we show the isochrones varying in metallicity for a single 10 Gyr age at *VIJHK* wavelengths. These wavelengths correspond to those for which we have data in the LMC, SMC, and IC 1613, which we turn to in Section 3 below.

We note here that the *I*-band magnitude is remarkably constant over this illustrated range of metallicities (and corresponding colors), and gives rise to a single (standard candle) *I*-band tip magnitude, while at other wavelengths there is instead a slanting distribution, or a (decreasing and/or increasing) "run" of absolute magnitudes with increasing metallicities/colors. There is therefore no unique "tip" magnitude in these other bands, but there is nevertheless a very well-defined (and theoretically predicted) correspondence of absolute magnitude with intrinsic color. We refer to these distributions as "TRGB sequences." The same stars defining the TRGB at a given metallicity will also define the tip in different band color–magnitude diagrams (CMDs), not at arbitrary magnitudes, but in the logical order that is predicted by the models. Moreover, the fact that higher metallicity manifests itself by making stars observed in the optical fainter while simultaneously resulting in brighter stars in the near-infrared, allows for the effects of metallicity and reddening to

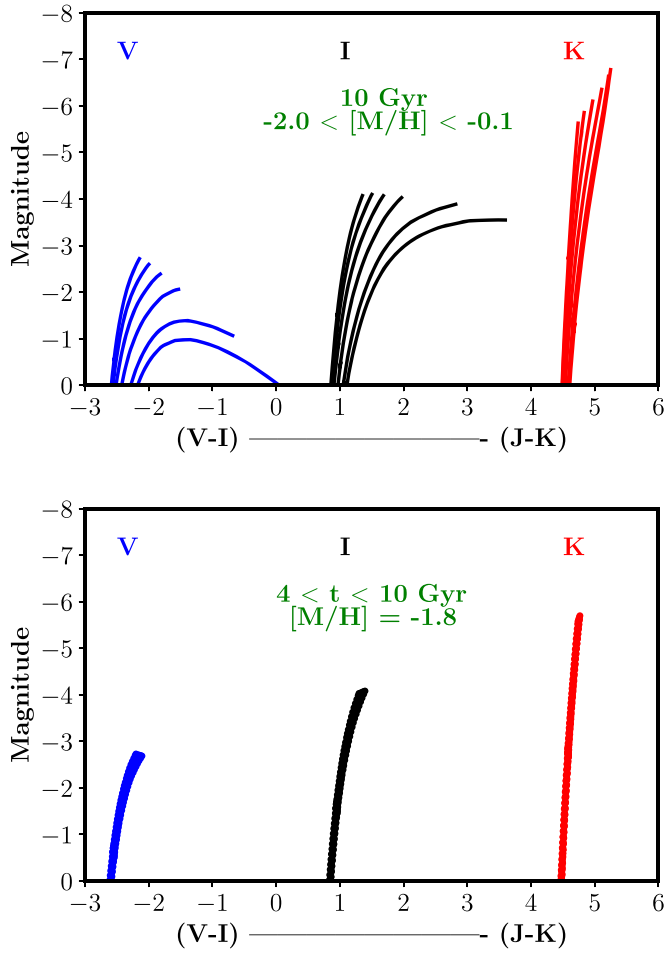

Figure 1. PARSEC isochrones for red giant branch (RGB) stars with a constant age and a metallicity spread (upper panel) and a constant metallicity, but with an age spread (lower panel), shown for V (blue), I (black), and K (red) bandpasses, to the same scale, for comparison. In the upper panel, the isochrones have a constant age of 10 Gyr and a metallicity range from $-2.0 < [M/H] < -0.1$ dex; in the lower panel, the isochrones have a fixed metallicity of $[M/H] = -1.8$, and an age spread of $4 < t < 10$ Gyr. The x-axis for the V and I isochrones is the $(V - I)$ color, while for K it is $(J - K)$; however, for clarity the V-band isochrones have been shifted by -3.5 mag in $(V - I)$, and the K-band isochrones have been shifted by $+4.0$ mag in $(J - K)$. As can be seen, for older stellar populations (>4 Gyr), the RGB colors are very insensitive to age, while the colors track differences in metallicity very clearly.

be decoupled and individually solved for. This direct dependence of the TRGB color with metallicity, and the negligible dependence on the age for older populations, provide a powerful means of accounting for differences in metallicity, while simultaneously correcting for extinction.

To summarize this section, there is little dependence on age for all TRGB stars older than about 4 Gyr (e.g., Serenelli et al. 2017). Conversely, there is an extremely tight relation between the color of the stars defining the TRGB and the metallicity of the TRGB population, which provides a basis to empirically measure the extinction.

In what follows, we do not use the theoretical isochrones in our analysis to determine reddenings or distances: we undertake an entirely empirical analysis. However, we confirm empirically that the behavior of the RGB with color and wavelength follows the general predictions from theory, thereby lending confidence to the overall method and its application.

3. The Methodology: A Multi-wavelength Approach to the TRGB Calibration

In this paper, we use *VI* photometric data from the third phase of the Optical Gravitational Lensing Experiment (OGLE-III; Udalski et al. 2008) for both the LMC and the SMC. For the LMC, we use the "Shallow" survey data published by Ulaczyk et al. (2012); the LMC and SMC data are available at the following website http://www.astrouw.edu.pl/ogle/ogle3/maps/. Y19 have pointed out that the coarser pixel scale in the optical (*UBVI*) survey of the two Magellanic Clouds undertaken by Zaritsky et al. (2002, 2004) probably suffer from blending issues. While the Zaritsky data for the SMC (but not the LMC) were used in the analysis by Freedman et al. (2019), here we now self-consistently use only the OGLE-III data for both the LMC and the SMC. In the near-infrared, *JHK* observations of both clouds were obtained in the course of the 2MASS all-sky survey. We have cross-identified the LMC and SMC stars from the OGLE-III surveys with those in 2MASS. This merged catalog forms the basis for the following study and the LMC calibration of the TRGB. The IC 1613 data analyzed in this paper are from Hatt et al. (2017).

The method that we are using is conceptually very simple. As noted above, the individual stars that define the tip in the I band (at 8000 Å) are precisely the same stars that must also define the TRGB at both shorter and longer wavelengths. Using a set of TRGB stars defined in the I band, we then make use of those same stars at a range of wavelengths from the optical to the near-infrared, where the extinction decreases with increasing wavelength. The overall methodology is similar in concept (but not identical) to that developed in the past for determining extinctions to Cepheid variables (e.g., Freedman 1988, Freedman et al. 1991).

Before proceeding further we note that in this study we confine ourselves to the color range $1.4 < (V - I) < 2.2$ mag $(-1.4 > [Fe/H] > -0.6)$, where the I-band magnitude of the TRGB is observed to be approximately constant (see Freedman et al. 2019 and references therein). At colors beyond this range the *theoretical dependence* of the I-band TRGB is nonlinear, as illustrated in Figure 3 of Mager et al. (2008) (which, in turn, was derived from Bellazzini et al. 2001; Bellazzini 2008); however, the color range specified above encompasses virtually all of the low-metallicity halo stars used in extragalactic distance determinations, and it symmetrically straddles the peak of the Bellazzini relation in that color range. For all practical applications the TRGB I-band magnitude (in that restricted color range) is effectively constant, the formal scatter being less than ± 0.01 mag (deviating by only ± 0.015 mag, peak-to-peak).

3.1. Schematic Illustration of the Method

In Figure 3, we show a schematic representation of the steps involved in measuring both extinction and reddening. The upper dashed lines represent the run of the TRGB absolute magnitude as a function of intrinsic color. The I-band relation is flat with color. The brightest RGB stars decline in luminosity as a function of color for wavelengths shorter than the I band, while these same stars increase in luminosity with color for wavelengths longer than the I band. The solid lines (marked "True") midway down in each of the three diagrams are the intrinsic TRGB sequences displaced to fainter magnitudes by identical (true distance modulus) offsets labeled μ_o. Further downward displacements of the TRGB lines are tagged by the

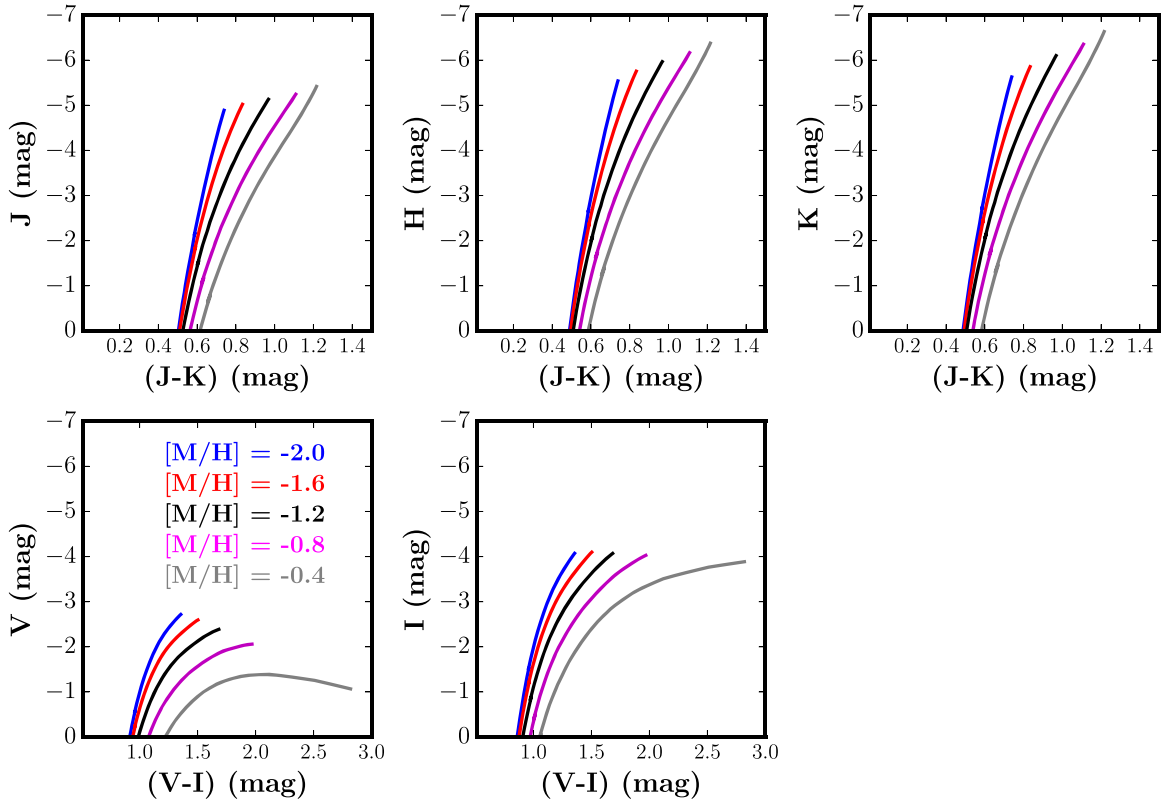

Figure 2. PARSEC isochrones for a single 10 Gyr age at *VIJHK* wavelengths. The isochrones span a range of metallicities of $-2.0 < [M/H] < -0.4$ dex. These bandpasses correspond to those in the observed color–magnitude diagrams for the LMC, SMC, and IC 1613 shown in Figures 5 and 6. These isochrones show the well-known behavior of the TRGB stars as a function of wavelength: the tip stars increase in brightness in the infrared; they are nearly constant in the *I* band, and they decrease in the *V* band.

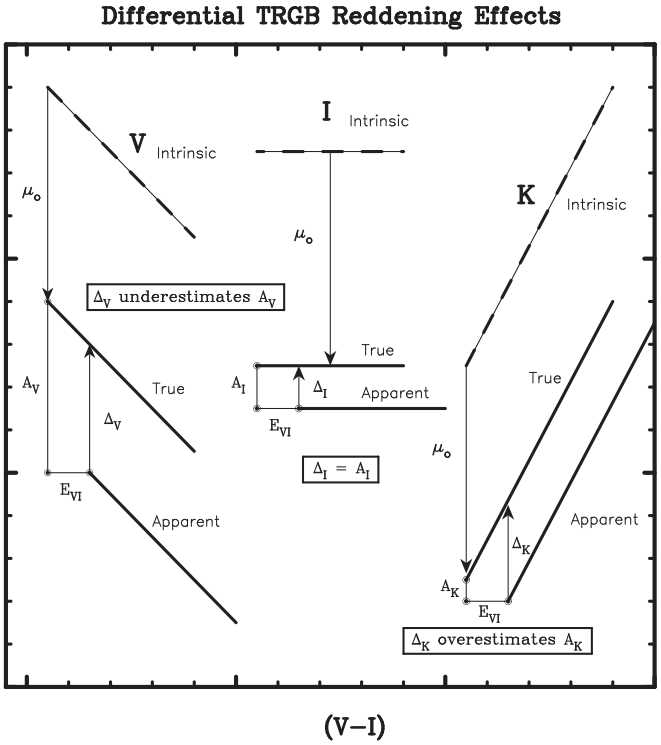

Figure 3. Schematic illustration of multi-wavelength TRGB seen in three representative bands labeled *V*, *I*, and *K* from left to right, illustrating the effects of distance, extinction, and reddening. See the text for details.

wavelength-dependent extinctions (A_V, A_I, and A_K) which systematically decrease in amplitude with wavelength, followed by wavelength-independent reddenings, each of the same amount, shown as $E(V-I)$ in each diagram. The resulting extincted, reddened, and distance-modulus-displaced traces of the three example TRGBs are labeled "Apparent." The upward arrows separating the "Apparent" and "True" moduli in *V*, *I*, and *K* have magnitudes of Δ_V, Δ_I and Δ_K as marked. It should be noted that *these vertical displacements are not to be confused or directly equated with the extinction values appropriate to each of those wavelengths, except for the I band where, coincidentally, the slope of the TRGB is flat with color*. For all downward-sloping ("blue") TRGB relations Δ_λ underestimates A_λ, and for all upward-sloping and ("infrared") TRGB relations Δ_λ overestimates A_λ. The magnitude of that error (the difference between A_λ and Δ_λ) is simply $s_\lambda \times E(V-I)$, where s_λ is the slope of the TRGB in the selected CMD. For clarity, $\mu_\lambda = \mu_o + \Delta_\lambda - s_\lambda \times E(V-I)$.

Using simulated error-free data, Figure 4 illustrates the method for using TRGB data to simultaneously determine the true distance modulus and, simultaneously, the total line-of-sight extinction and reddening from multi-wavelength data. The steep solid line (labeled True) is the run of extinction as a function of wavelength fit to the observations. Scatter around this particular fit is, by definition, zero for this simulated set of error-free data. The apparent magnitude off-sets Δ_λ between the intrinsic and the apparent TRGB relations (as described in Figure 3) are shown as squares with inset filled circles. They show a shallow run of extinction with wavelength that is significantly less than the input value, and they show

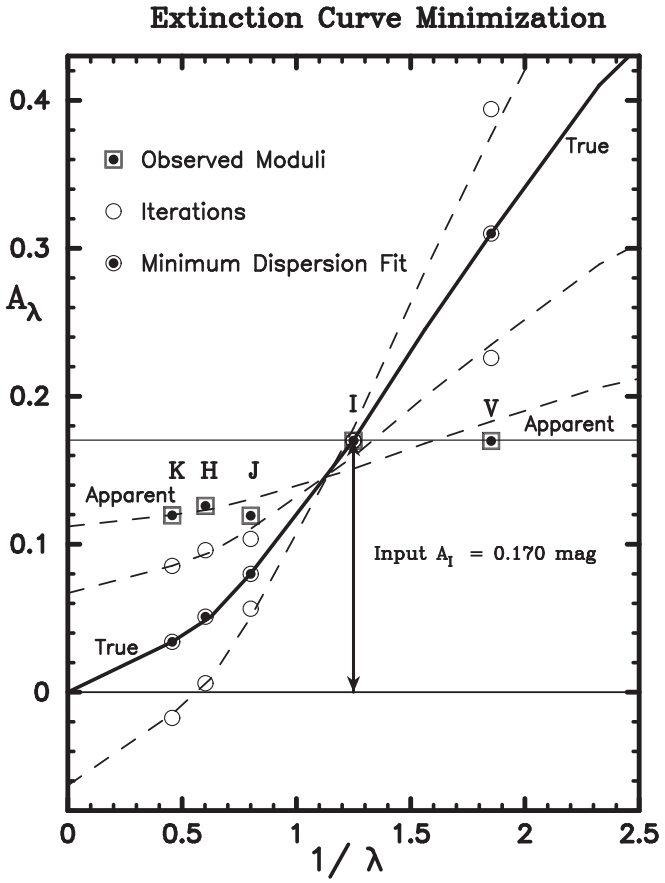

Figure 4. Schematic illustration of the process of using TRGB data to simultaneously determine the true distance modulus and reddening from multi-wavelength data. Dots enclosed in squares are the result of the first iteration on the reddening simply differencing the apparent magnitude of the tip stars with the intrinsic relations. The scatter is non-negligible. Open circles show alternative reddening solutions on both sides of the input value. These solutions also show increasing (non-zero) scatter, most easily seen in the dashed-line solutions passing above and below the *I*-band data point. The input reddening is shown by the circled dots and fit by the steep solid line which was recovered by simply mimimizing the dispersion about the fit. See the text for details.

measurable scatter, resulting from not having applied the shifts required by the reddening terms. By iteratively compensating for the difference between Δ_λ and A_λ, re-plotting, re-fitting, and each time re-calculating the sum of the squares of the residuals, a minimum is approached and then exceeded (when the applied reddening exceeds the input value), as illustrated by the two surrounding solutions in Figure 4 (which have measurable scatter clearly in excess of zero) shown as dashed lines through open circles.

3.2. Application of the Method

We begin with the I versus $(V-I)$ CMD where the slope of the TRGB is minimally impacted by color/metallicity variations, as noted above. The full set of CMDs for the OGLE-III LMC data is shown in Figure 5. For the LMC we spatially restricted the CMD sample to those stars *outside* of a one-degree radius circle centered on the bar of the LMC, where crowding within the high-surface-brightness (high-crowding) portions of the bar could bias the magnitudes of the TRGB stars therein.

The I versus $(V-I)$ CMD is shown in the upper right panel. We selected a small subset of 306 tracer stars in the CMD that fall symmetrically about the calibrated fit to the tip, selected within the color range $1.4 < (V-I) < 2.2$ mag. These stars have OGLE *I*-band photometry (as noted above, from the "Shallow" survey data published by Ulaczyk et al. 2012), with quoted errors of less than ± 0.02 mag at $I \sim 14.5$ mag. They sample the tip with a scatter of ± 0.04 mag, giving a scatter on the mean of ± 0.002 mag. In the optical, the slope in the *I*-band has been set to zero (thereby resulting in a *V*-band slope of unity), while in the near-infrared the slopes are taken from Madore et al. (2018). We give these here for completeness, along with their uncertainties: at J, H, and K, the slopes are -0.85 ± 0.09, -1.62 ± 0.16, and -1.85 ± 0.19, respectively. Our specific goal here is the difference in zero-points, not a full solution of all possible parameters. As we shall see, these slopes are consistent with the observed CMDs shown in Figures 5 and 6 discussed below. Thus we solve here for two parameters only: the total line-of-sight reddening and the true distance modulus for our selected sample of LMC TRGB stars.

Given the set of tracer stars described above (taken from Freedman et al. 2019 and derived from their Figure 4), we mapped each of the *I*-band tracers into the CMDs at shorter (V) and longer (JHK) wavelengths. Using the adopted slopes of the TRGB in the flanking CMDs shown in Figure 5, we then determined their individual zero-points by minimizing the scatter between the intrinsic line of pre-determined slope and the tracer stars. Errors on the mean for each of the zero-points were then calculated from the measured scatter of the 306 tracer stars in each color.

For our TRGB zero-point calibration via the LMC, we use two fiducial galaxies, IC 1613 and the SMC, each with very low line-of-sight reddenings. Before undertaking the multi-wavelength, differential reddening analysis of the TRGB population of the LMC with respect to these galaxies, we first subtracted the small foreground reddenings of $E(B-V) =$ 0.022 (IC 1613) mag and 0.033 mag (SMC), respectively, based on the Galactic foreground reddening maps of Schlafly & Finkbeiner (2011), which is a re-calibration of Schlegel et al. 1998), as tabulated in NED. To be clear, these maps do not include any correction for extinction in the main bodies of galaxies along the extended line of sight, but the host-galaxy TRGB stars are expected to have negligible extinction, given that they reside in the gas- and dust-free halos of these galaxies. In Figure 6, we show a similar set of the five *VIJHK* CMDs for IC 1613 and the SMC. The fits to their TRGB sequences were obtained using the identical procedure as discussed above for the LMC stars. Subtracting the respective fits at each of the wavelengths for both galaxies, we determined differential apparent distance moduli to our subset of TRGB stars in the LMC for each of the five ($VIJHK$) bandpasses. This step yields a first estimate of the differential distance moduli, each of which contains a fixed pillar, which is the difference in their true moduli. This common (geometric) offset is, of course, independent of wavelength. We emphasize, however, that these simple differential distance moduli at this stage do not yet account for the *reddening* of the TRGB stars, and they are therefore only a first approximation to the *extinction*. As we describe below, to measure *both extinction and total reddening* we iterate on the solution, solving simultaneously for distance, extinction and reddening by minimizing the sum of the squares of the residuals around the fit of extinction versus inverse wavelength. In what follows, we have adopted the reddening curve used in NED which is taken from Schlafly & Finkbeiner

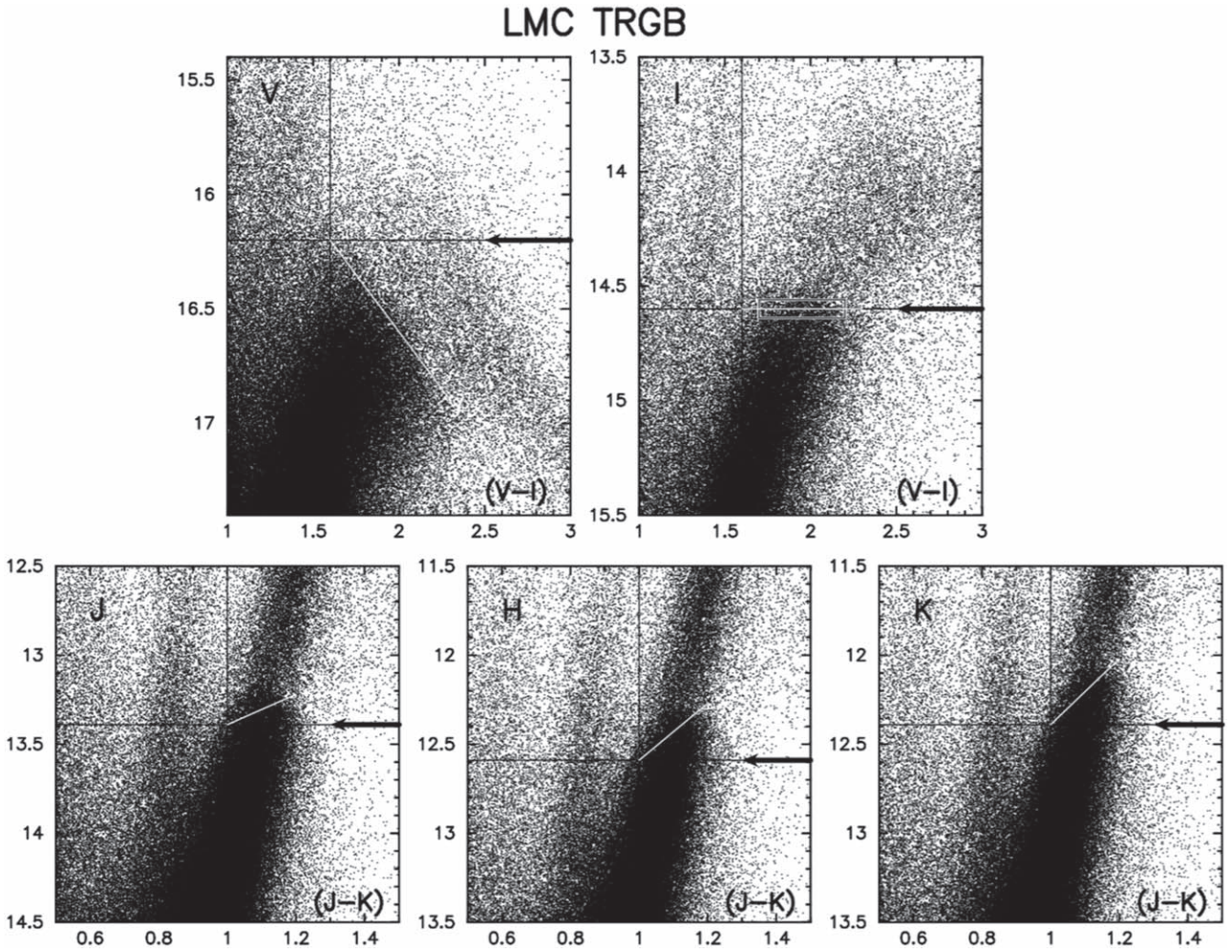

Figure 5. Color–magnitude diagrams (CMDs) for the RGB population of stars outside of the bar region of the LMC. The two plots across the top are for the optical (*VI* bandpass and $(V-I)$ colors from OGLE-III), while the three across the bottom are for the near-infrared (*JHK* bandpass and $(J-K)$ color from 2MASS). All of the panels are zoomed into a two-magnitude vertical luminosity range and a lateral range in color of 2.0 mag in $(V-I)$ for the optical, and 1.0 mag in $(J-K)$ for the near-infrared. The white lines mark the apparent magnitude level of the TRGB at each of the wavelengths, using predetermined slopes, fit to the data as described in the text. Arrows indicate the magnitude level in each bandpass at which the color calibration of the TRGB is normalized (i.e., at $(J-K)=1.00$ mag for *JH* and *K*, and at $(V-I)=1.80$ mag in *V* and *I*. The *I*-band selection function for the tracer stars is outlined by the white rectangle centrally located in the upper right CMD.

(2011), which in turn is derived from Fitzpatrick (1999) using $R_v = 3.1$. We have used a source spectrum appropriate to a K-type giant, closely matching a typical elliptical galaxy or, as in this case, TRGB stars.

3.3. Extinction Curves

In Figure 7 (lower panel) we show the iterated extinction plot derived from a comparison of the apparent magnitudes of the TRGB stars in the LMC with respect to IC 1613. The fit, as shown by the solid black line, gives a difference in their true distance moduli of $\Delta\mu = +5.899$ mag, giving a true distance modulus for IC 1613 of $\mu_{\rm IC1613} = 24.376$ mag. This distance agrees reasonably well with the recently published Cepheid distance modulus of 24.29 ± 0.03 mag given by Scowcroft et al. (2013). (The mean and median of the 22 TRGB independently determined values cited in NED are 24.340 and 24.365 mag, respectively.) The line-of-sight reddening to the LMC TRGB stars, using IC 1613 as the calibrator, gives for the LMC $E(B-V) = 0.094$ mag ($A_I = 0.160$ mag) which compares favorably to the value of $A_I = 0.169$ mag derived below using the SMC. These values agree to within 0.001–0.002 mag with those given in Freedman et al. (2019); the small difference arises because a larger comparison sample of LMC stars (306 versus 200) was used in the current analysis.

Next we use the SMC as the normalizing source for a comparison with the LMC, which gives an independent run of extinction with inverse wavelength for the LMC stars, as shown in the lower panel of Figure 7. Here we derive a difference in the true moduli of $\Delta\mu({\rm SMC}-{\rm LMC}) = 0.474$ mag and a reddening to the TRGB stars in the main body of the LMC of $E(B-V)_{\rm LMC} = 0.100$ mag ($A_I = 0.169$ mag). These values can be compared to the preliminary values in Freedman et al. (2019): $\Delta\mu({\rm SMC}-{\rm LMC}) = 0.484$ mag; $E(B-V)_{\rm LMC} = 0.093$ mag; ($A_I = 0.158$ mag). Here we adopt the NED foreground reddening to the SMC. We note that the reddening value given in Freedman et al. (2019) was $E(B-V)_{\rm LMC} = 0.093$ mag, and differs primarily as a result of our current adoption of the OGLE-III data for the SMC rather than the photometry from Zaritsky et al. (2002).

It should be noted that the two unknowns (true distance modulus and reddening) cannot (mathematically) be determined

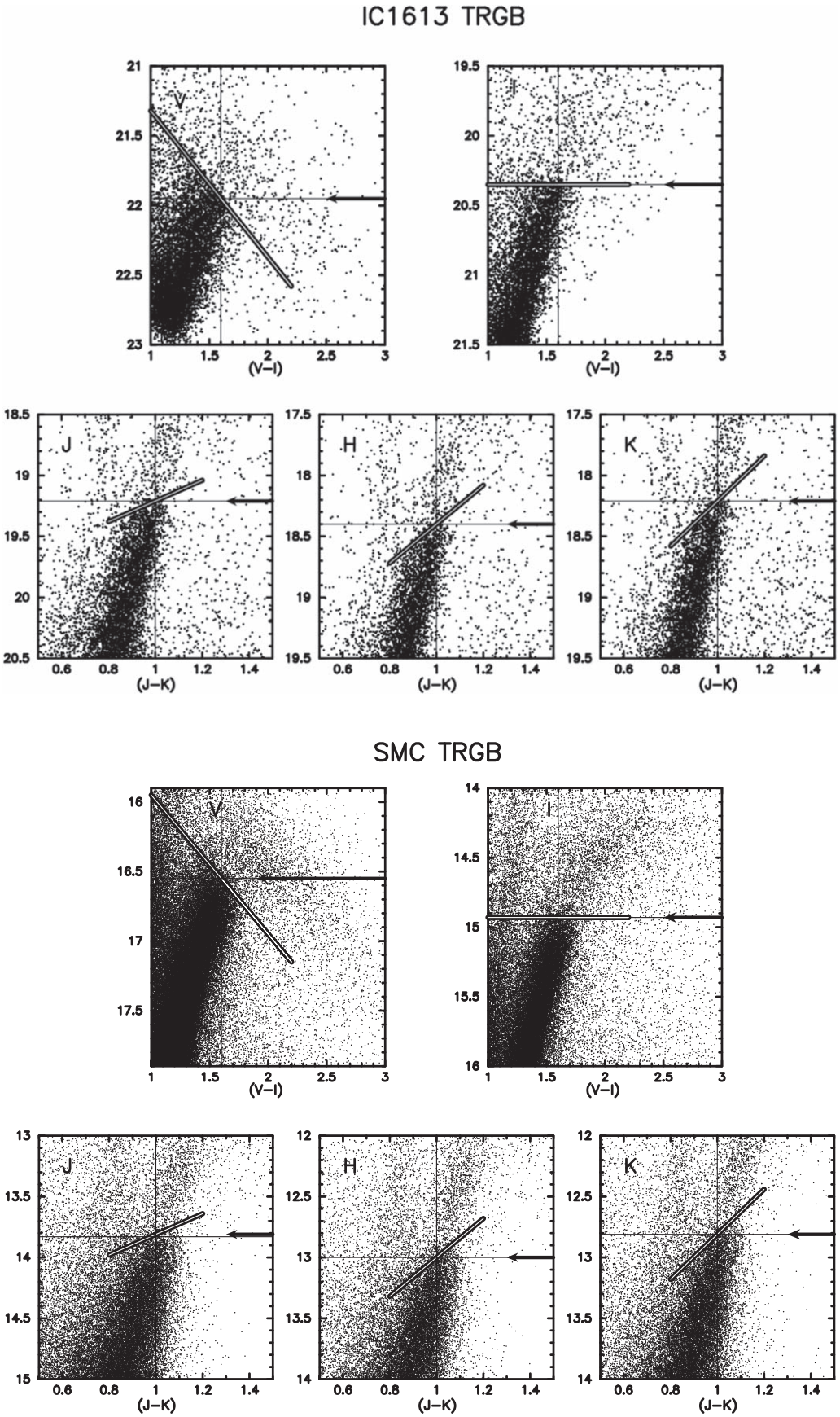

Figure 6. CMDs for the RGB population of stars in IC 1613 (top five) and the SMC (bottom five). The two across the top of each montage are for the optical (*VI* bandpass, and $(V-I)$ colors), while the three across the bottom are for the near-infrared (*JHK* bandpass, and $(J-K)$ colors, from 2MASS). The IC 1613 data are from Hatt et al. (2017) and the SMC optical data are from OGLE-III. The slanting lines mark the apparent magnitude levels of the TRGB at each of the wavelengths, using predetermined slopes, and fit as described in the text. The arrows are as described in Figure 5.

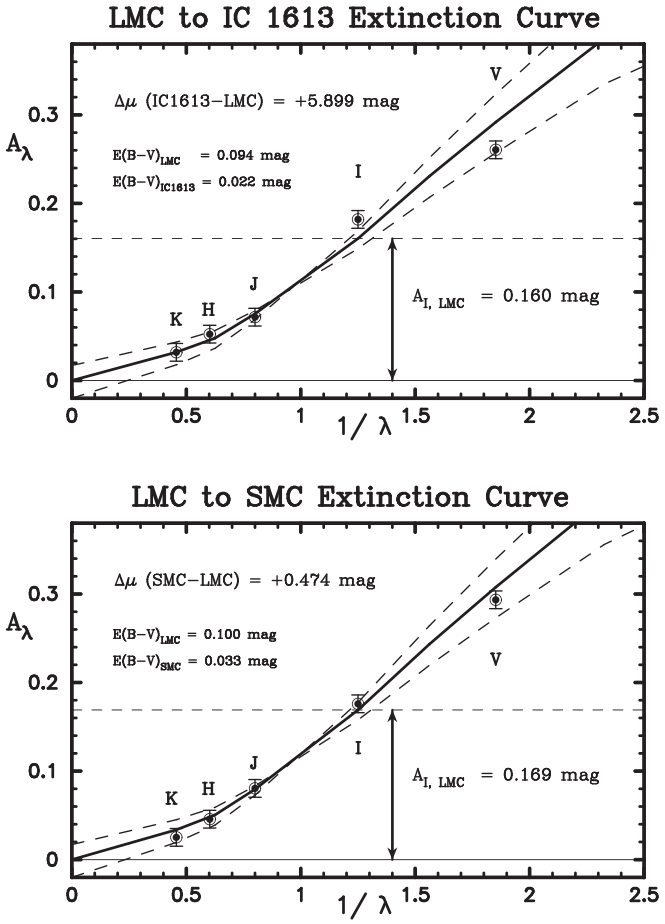

Figure 7. Run of apparent differential distance modulus measured at five wavelengths (*VIJHK*) for LMC TRGB stars with respect to IC 1613 and the SMC in the upper and lower panels, respectively. The upward trending solid lines are Galactic extinction curves fit to the data where for the LMC $E(B-V) = 0.094$ mag for the LMC adopting $E(B-V) = 0.022$ mag (from NED) for IC 1613 (upper panel); and $E(B-V) = 0.100$ mag with $E(B-V) = 0.033$ mag (from NED) for the SMC (lower panel), as described in the text.

from one pair of colors. At least three bands (two independent colors) are required. If this minimal number is adopted in future studies, then as large a wavelength baseline as possible should be chosen. With current facilities *V*, *I*, and *K* bands would be a competitive choice.

3.4. Zero-points

We take the DEB distance modulus to the LMC to be 18.477 mag (Pietrzyński et al. 2019). Taking the average of the two LMC reddenings derived above then gives $E(B-V)_{\rm LMC} = 0.097$ mag, which converts to $A_V = 0.300$, $A_I = 0.165$, $A_J = 0.078$, $A_H = 0.049$, and $A_K = 0.032$ mag. Applying these corrections to the observed magnitudes of the TRGB stars in the LMC at their respective wavelengths gives the following absolute multi-wavelength calibrations of the TRGB method normalized to an intrinsic color of $(V-I)_o = 1.80$ mag and applicable over the color range $1.4 < (V-I)_o < 2.2$ mag for the optical (*VI*), and normalized to $(J-K)_o = 1.00$ mag for the near-infrared (*JHK*) calibration. In updating our calibration with respect to earlier ones we have here rationalized the pivot-point colors in the optical and infrared so that the fits in both

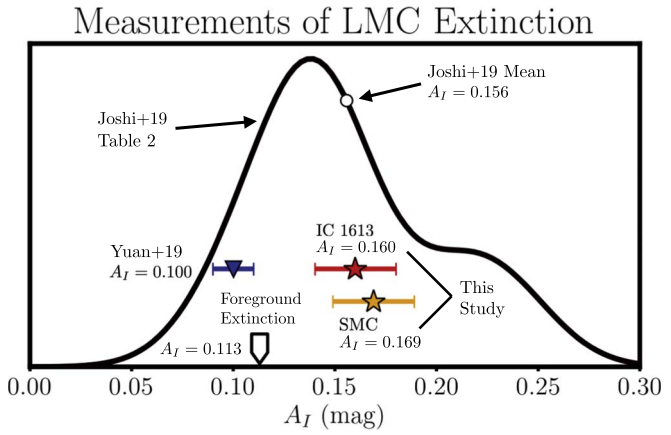

Figure 8. Smoothed histogram of reddening values found in Joshi & Panchal (2019), their Table 2, converted to extinctions adopting a Fitzpatrick (1999) reddening law (solid black line). These extinction values are determined for a variety of stellar populations. The mean of the distribution is shown by an open white circle. In blue is the extinction value suggested by Yuan et al. (2019; Y19), based on a crowding correction, applied to the SMC photometry of Zaritsky et al. (2002). See the Appendix for a detailed description of why this post-processing of the results presented in Freedman et al. (2019) is problematic. In red and orange are the values determined here for TRGB stars, using IC 1613 or the SMC, respectively, to set the reddening floor. These values agree at the millimag level with the equivalent measurements made in Freedman et al. (2019). For reference, the thick white arrow plotted is the Schlafly & Finkbeiner (2011) estimate of the foreground reddening to the LMC. We note that the *total* extinction adopted by Y19 is smaller than the foreground extinction. The two LMC extinctions derived in this paper, using the SMC and IC 1613, are shown as orange and red stars, respectively, and highlighted by two lines pointing to the label "This Study."

cases are set to colors that correspond to the same metallicity, i.e., [Fe/H] = −1.0 dex. This simply requires moving the $(V-I)$ normalization from 1.60 to 1.80 mag. This shift does not impact the *I*-band calibration, which is taken to be flat over the above color range. For the *I* band, $M_I^{\rm TRGB} = 14.595 - 18.477 - 0.165 = -4.047 \pm 0.022$ (stat) $\pm$ 0.039 (sys) mag, where the uncertainties are summarized in Table 2 of Freedman et al. (2019).

The difference in the current $(V-I)$ calibration from that given in Freedman et al. (2019) is due to the small shift in M_I from −4.04 (see the Appendix in Freedman et al.) to −4.05 mag, and re-centering on $(V-I) = 1.80$ mag instead of 1.6 mag. The difference in the current $(J-K)$ calibration from that given in Freedman et al. (2019) is due to moving away from the LMC bar to a new outer annulus sample of stars, and ensuring that the M_J and M_K zero-points differ by exactly 1.00 mag:

$$M_V = -2.25 + 1.00 \times [(V-I)_o - 1.8]$$
$$M_I = -4.05 + 0.00 \times [(V-I)_o - 1.8]$$
$$M_J = -5.14 - 0.85 \times [(J-K)_o - 1.0]$$
$$M_H = -5.95 - 1.62 \times [(J-K)_o - 1.0]$$
$$M_K = -6.14 - 1.85 \times [(J-K)_o - 1.0].$$

3.5. Discussion of Published LMC Reddenings

Joshi & Panchal (2019) have recently provided a summary of published spatial extinction maps for various populations of stars in the LMC (see their Table 2). In Figure 8, we show a smoothed representation of these published extinction values, which range from $A_I = 0.10$ to 0.24 mag, after incorporating

the DEBs at the midpoint of the range of values provided. From a kernel density estimation, the mode of the *I*-band LMC extinction values is estimated to be $A_I = 0.138^{+0.074}_{-0.029}$ mag (68% CL). Our value lies close to both the mean and the mode of the distribution. We note that the range of values of $A_I = 0.094$–0.109 mag, chosen by Y19 for the LMC extinction, falls very near the lower bound on the extinction values quoted by Joshi & Panchal, based on the Haschke et al. (2011) study. In their Section 4.1, Y19 quote an uncertainty ± 0.03 mag (smaller than the uncertainty of 0.07 mag, quoted in the original Haschke et al. study), which renders this discrepancy even more significant. Finally, we further point out that the Y19 adopted value falls below the average foreground extinction of $A_I = 0.113$ mag along the line of sight to the LMC (Schlafly & Finkbeiner 2011).

4. Consistency Checks on the TRGB Calibration

4.1. DEB Distance to the SMC

Graczyk et al. (2014) used five DEBs in the SMC to determine the differential distance between the two clouds deriving a value of $\Delta\mu$(SMC–LMC) = 0.472 mag ± 0.025 mag (lower limit based on the SMC uncertainty alone) using an older DEB distance to the LMC. Each of the individual DEB measurements have a typical quoted uncertainty of ±0.03 mag. Updating to the most recent LMC DEB distance scale of $\mu_o = 18.477 \pm 0.026$ mag (Pietrzyński et al. 2019), this gives $\Delta\mu(\mathrm{SMC} - \mathrm{LMC}) = 0.488 \pm 0.036$ mag, which is within half a sigma of our independent determination of 0.474 mag, as given above. (See Pietrzyński et al. 2019 for a recent and detailed discussion of the DEB method as applied to the calibration of the extragalactic distance scale.) Updating the Y19 calculation in their Section 4.2 increases the extinction to the LMC to $A_I = 0.125$ mag, and places it beyond the 3σ contours of their Figure 10 solutions.

Adopting $\Delta\mu$(SMC–LMC) = 0.488 mag and the DEB distance modulus for the SMC of 18.965 ± 0.025 (stat) ± 0.048 (sys) mag, our detection of the *I*-band TRGB at 14.93 mag and an extinction of $A_I = 0.056$ mag (NED) gives M_I(SMC) = −4.09 ± 0.03 (stat) ± 0.05 (sys) mag, in systematic agreement, at the one-sigma level, with our LMC measured value of −4.05 ± 0.03 (stat) ± 0.05 (sys) mag. The SMC tip detection was made using a standard Sobel filter applied to a GLOESS-smoothed *I*-band luminosity function based on stars within the color range $1.4 < (V - I) < 1.8$ mag, using software and methods identical to those used in Freedman et al. (2019). Within that same color range 138 tip tracer stars, used to measure the tip magnitudes in *VJH* & *K*, yielded an error on the mean of $\sigma_{I(\mathrm{TRGB})} = \pm 0.007$ mag.

4.2. DEB-based Galactic Globular Cluster Calibration of the TRGB

We now present a second independent check on the calibration of the TRGB. The zero-point of this calibration of the near-infrared TRGB is based upon the recently measured DEB-based geometric distance to 47 Tucanae (Thompson et al. 2020).[8]

Following DCA90 we use a selection of Galactic globular clusters, covering a wide range of metallicities ([Fe/H] = −2.2 to −0.7)[9] to produce multi-wavelength (*JHK*) composite CMDs. The composite CMD can then serve as the basis for an independent check on the zero-point calibration of the TRGB sequences, for comparison with the mixed-metallicity populations seen in the halos of nearby galaxies. Our sample includes M2, M4, M5, M15, M55, NGC 0362, NGC 1851, NGC 6362, NGC 6397, NGC 6752, and 47 Tuc. We use the DCA90 compilation because it provides a set of consistent *relative* distances to the various clusters. We set the absolute zero-point using the recently determined DEB measurements. In a more detailed, multi-wavelength study of the TRGB calibration in preparation, we will be applying proper-motion selection using high-resolution *Gaia* DR2 data to study a significantly larger sample of 45 Galactic globular clusters (observed in 10 bandpass from the optical to the near-infrared).

At present, we have revisited the TRGB calibration of the slopes and zero-points primarily in the near-infrared for two main reasons. (1) There is homogeneous, high-precision, and high-accuracy *JHK* photometry for all of these targets, obtained in the course of the 2MASS all-sky survey (Cutri et al. 2006).[10] (2) The impact of line-of-sight reddening on the zero-point calibration of the TRGB is greatly diminished by working in the infrared. The globular cluster sample studied by DCA90 is a relatively low line-of-sight reddening subset of Galactic globular clusters, with reddenings ranging from $E(B - V) = 0.02$–0.10 mag, which translate to extinction corrections in the near-infrared of $A_J = 0.016$–0.080 mag, $A_H = 0.01$–0.05 mag and $A_K = 0.007$–0.034 mag (after dropping NGC 6397 because of its large foreground extinction of $A_V = 0.56$ mag.) Reddening corrections have been adopted from DCA90. We note also the *JHK* TRGB study for 24 globular clusters belonging both to the bulge and the halo of the Galaxy, undertaken by Valenti et al. (2004a, 2004b). In general the reddenings for this sample are larger (with $E(B - V)$ values up to 1.3 mag), so we have not (at this time) used them for our purposes.

4.2.1. 47 Tucanae

Thompson et al. (2020) have determined direct distances to two DEBs in the metal-rich Galactic globular cluster 47 Tuc. These two stars have geometrically determined distances of 4.41 ± 0.06 and 4.60 ± 0.09 kpc, respectively, giving an average true distance modulus of $\mu_o = 13.27 \pm 0.07$ mag. As noted in Thompson et al., the analysis by Chen et al. (2018) of *Gaia* parallaxes to 47 Tuc yields a distance modulus of 13.24 ± 0.005 (stat) ± 0.058 mag (sys). The *Gaia* parallax corresponds to a distance of 4.45 kpc, which agrees with the DEB distance to within 1%. Adopting the DEB geometric calibration, we re-zero the true distance moduli to each of the DCA90 globular clusters, with the required offset being −0.12 mag.

4.2.2. Composite Globular Cluster CMDs and Luminosity Functions

In Figure 9 we show a composite *JHK* CMD which combines each of the individual data sets for the least-reddened

[8] We note that, in general, the limitation of measuring the TRGB in individual globular clusters is the small numbers of stars populating the tip. These measurements can, however, serve to provide a firm lower limit to the tip magnitude. However, in the more populated clusters (e.g., 47 Tucanae and ω Cen), the numbers are large enough to provide calibrations in their own right.

[9] As compiled by Harris (1996, 2010 edition): http://physwww.mcmaster.ca/~harris/mwgc.dat.

[10] These data are publicly available through *IRSA* at https://irsa.ipac.caltech.edu/cgi-bin/Gator/nph-dd.

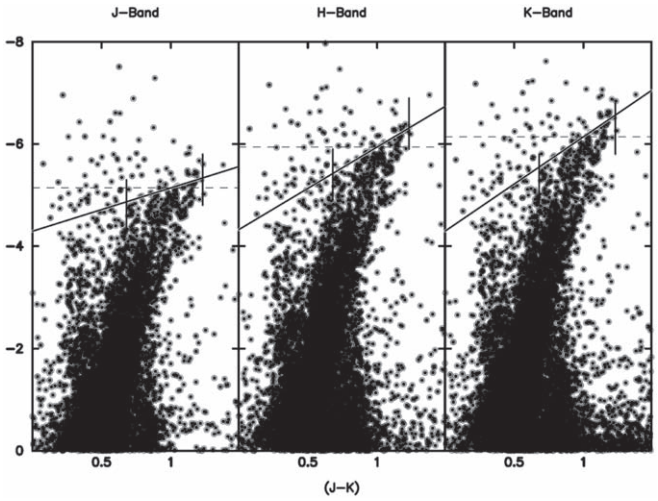

Figure 9. Composite CMD for the 11 Galactic clusters. The upward-slanting lines are fits to the TRGB sequences in Madore et al. (2018), as described and updated in the text. The dashed line is the fiducial magnitude read off at $(J-K)_o = 1.00$ mag. The vertical lines at $(J-K) = 0.7$ and 1.2 mag mark the color range within which the linear approximation to the TRGB sequence holds observationally.

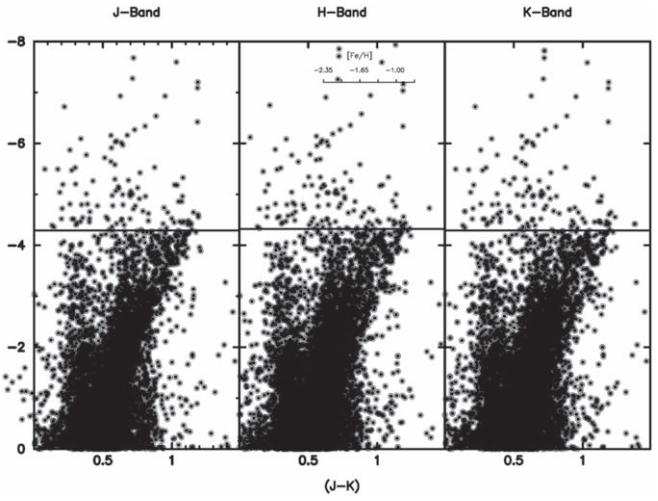

Figure 10. Composite CMD for the clusters shown in Figure 9, where in this case, the magnitudes have been rectified by flattening out the color dependence seen in the raw CMDs.

clusters. The upward-slanting lines in each of the three panels trace the TRGB calibration, previously published in Madore et al. (2018). The correspondence between the two provides an independent check and confirmation of the result derived from the LMC TRGB stars. The two vertical lines mark the intrinsic color range ($0.65 < (J-K) < 1.25$ mag) over which a linear calibration can be observationally defined. The horizontal broken line shows the magnitude of the TRGB increasing in brightness toward longer wavelengths as measured at the fiducial color of $(J-K) = 1.00$ mag.

Using the measured slopes we flatten or "rectify" the CMDs such that their marginalized luminosity functions show the greatest contrast in the TRGB discontinuity. The rectified CMDs are shown in Figure 10. Figure 11 shows the marginalized luminosity functions of the rectified composite CMDs for the Galactic globular clusters shown above. A total of 117 RGB stars contribute to the ± 0.3 mag interval within which the detection and measurement of the tip was made in this figure. The statistical uncertainty on the detections is found to be ± 0.051 mag in J and K and ± 0.057 mag in H. Averaged over the three wavebands, the derived zero-point in the I band is calculated to be $M_I = -4.056 \pm 0.053$ (stat) $\pm$ 0.080 (sys) mag, where the systematic error is that carried over directly from the DEB systematic error on the distance to 47 Tuc.

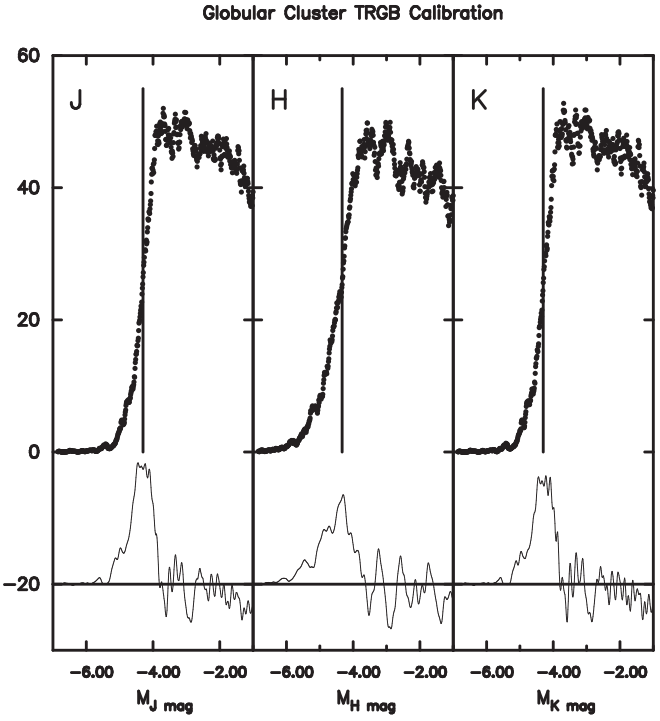

Figure 11. Galactic globular cluster edge-detector output. *JHK* luminosity functions for the rectified CMDs (using the Madore et al. 2018 slopes) (upper curves) and their corresponding edge-detector responses (lower curves) are given for a six-magnitude interval in luminosity, centered on the TRGB. See the text for more details.

4.3. Geometry of the LMC

A further test that we have undertaken is to determine the effect of geometry on the measurement of the TRGB in the LMC. Using the OGLE-III photometric data from Ulaczyk et al. (2012), we adopted a position angle of 132 deg and an inclination angle of 25 deg for the LMC disk, as determined by Pietrzyński et al. (2019) (see also Figure 3 of Jacyszyn-Dobrzeniecka et al. 2016, based on Cepheids). As these and earlier studies of the LMC have shown, the northeast side of the LMC is closer to us.

We calculated the displacements of individual stars along the line-of-sight direction between the tilted (observed) and non-tilted (inclination corrected) disks. The displacement is measured to be up to ~1400 pc (~3% in distance and ~0.06 mag in distance modulus). The median/mean of the displacements is very small, amounting to only ~10 pc. This is naturally expected, as the spatial coverage of the OGLE data is quite symmetric centered on the LMC. We then applied the edge detection algorithm to the original and the inclination-corrected OGLE catalogs. As can be seen in Figure 12, the two measured tip values are entirely consistent.

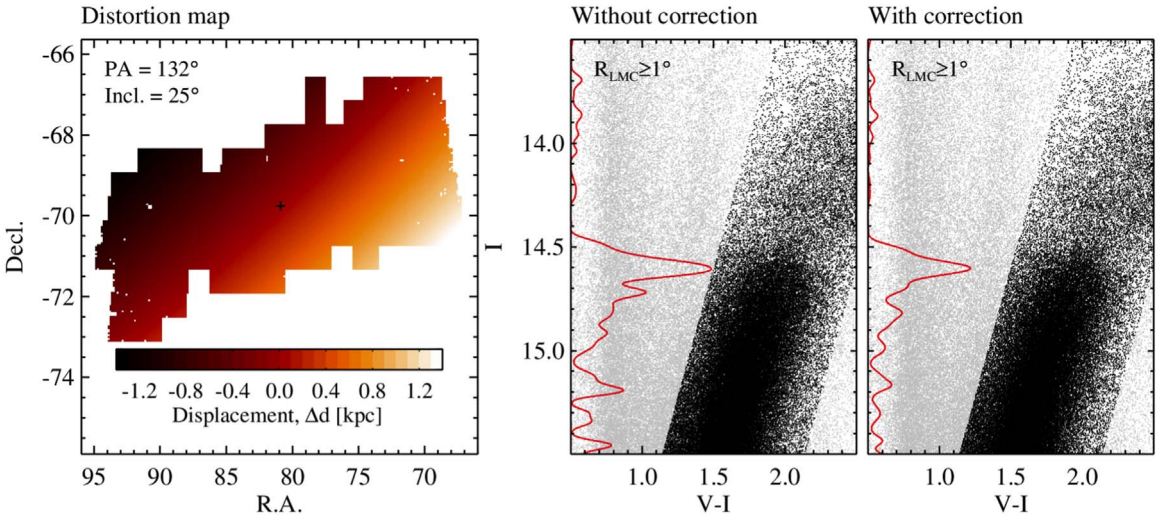

Figure 12. Test of the effects of geometry on measurement of the TRGB in the LMC. Left: a map showing the displacement ($\Delta d = d - d_{\rm corr}$) along the line-of-sight direction, as a result of the tilted LMC disk. We assume a position angle of 32 deg and an inclination angle of 25 deg (Pietrzyński et al. 2019) for the LMC disk plane. The mean of the displacement is only ∼10 pc. Right two panels: CMDs of the outer region of the LMC before (left) and after (right) the distortion correction. The measured TRGBs are almost identical (14.606 mag and 14.604 mag), respectively, indicating that the LMC disk geometry has no statistically significant impact on our TRGB measurement.

Table 1
TRGB Zero-points

Data	$M_I^{\rm TRGB}$	$\sigma_{\rm stat}$	$\sigma_{\rm sys}$	Notes
LMC	−4.047	0.022	0.039	Comparisons with IC 1613 and SMC
SMC	−4.09	0.03	0.05	SMC DEBs
Globular clusters	−4.05	0.05	0.08	47 Tuc DEBs + composite *JHK*

4.4. Summary of Consistency Checks on the Zero-point

As summarized in Table 1, the independent determinations of the *I*-band magnitude for the TRGB based on the (1) DEB measurements for the SMC and (2) *JHK* 2MASS observations for a sample of Galactic globular clusters, calibrated by DEB distance measurements in 47 Tucanae, agree very well with our determination for the LMC (see Section 3.4). We adopt the latter measurement, $M_I^{\rm TRGB} = -4.047 \pm 0.022$ (stat) $\pm$ 0.039 (sys) for our calibration of the TRGB. For clarity, we note that the calibration for the F814W filter, differs from the *I*-band calibration by −0.0068 mag (see Freedman et al. 2019, Section 3.4), giving $M_{\rm F814W}^{\rm TRGB} = -4.054 \pm 0.022$ (stat) $\pm$ 0.039 (sys).

5. Implications for the Hubble Constant

We adopt the average of our measured values from Section 3.4 of $A_I^{\rm LMC} = 0.165 \pm 0.02$ mag. Based on the calibration for *HST*/ACS F814W from Freedman et al. (2019), applied to a sample of nearby galaxies with TRGB distances, and tied to the Carnegie Supernova Project distant sample of SNe Ia, we determine a slightly revised value of $H_0 = 69.6 \pm 0.8$ ($\pm$1.1% stat) $\pm$ 1.7 ($\pm$2.4% sys) km s^{-1} Mpc^{-1}, (a difference of 0.23%). We note that, despite the criticisms leveled by Y19, our value of H_0 agrees to within 1σ with their quoted value of $H_0 = 72.4 \pm 1.9$. In Figure 13, we show our value of H_0 compared to other recently published determinations in the literature. Our purpose in this paper is not to undertake a detailed assessment of current H_0 values. At this time, we note simply that the Hubble "tension" issue remains.

6. Summary and Conclusions

In this paper we have introduced and described in detail a new methodology for the simultaneous determination of true distance moduli and *total* line-of-sight reddenings for TRGB stars, self-consistently using multi-wavelength data for the TRGB stars themselves. We have used a set of stars in the outer main body of the LMC, combined with the recently published high-accuracy and high-precision distance to the LMC, to calibrate the TRGB method at five independent wavelengths ranging from the optical (*VI*) to the near-infrared (*JHK*).

The multi-wavelength calibration resulting from the LMC analysis alone is given in Section 3.4. We find an absolute *I*-band magnitude for the TRGB of $M_I^{\rm TRGB} = -4.047 \pm 0.022$ (stat) $\pm$ 0.039 (sys); and for F814W, $M_{\rm F814W}^{\rm TRGB} = -4.054 \pm 0.022$ (stat) $\pm$ 0.039 (sys). Independent consistency checks on this calibration have also been presented. The first is a calibration through TRGB stars in the SMC, using a geometric distance to the SMC based on five DEBs. This calibration gives an *I*-band zero-point of $M_I = -4.09 \pm 0.03$ (stat) $\pm$ 0.05 (sys) mag. The second is a near-infrared calibration of using a composite set of Galactic globular clusters with a range of (spectroscopically determined) metallicities from [Fe/H] = −2.2 to −0.7 dex. Without any additional free parameters, we set the zero-point calibration adopting the new DEB distance modulus to 47 Tuc, tied to the relative distances from DCA90. This gives an *I*-band zero-point of $M_I = -4.06 \pm 0.05$ (stat) $\pm$ 0.08 (sys) mag. Each of these independent checks results in zero-points consistent with our adopted value of our primary calibration using the LMC alone.

We find a value for the LMC TRGB extinction of $A_I = 0.160 \pm 0.024$ mag using the nearby galaxy IC 1613, for the differential reddening comparison. This value agrees well with the independent value of $A_I = 0.169 \pm 0.014$ mag, using OGLE-III photometry for the SMC. This photometry suffers less from crowding/blending effects than that of Zaritsky et al. (2002), and leads to an improved estimate of the LMC TRGB extinction than that obtained by Freedman et al. (2019). Our measurement technique has the advantage of

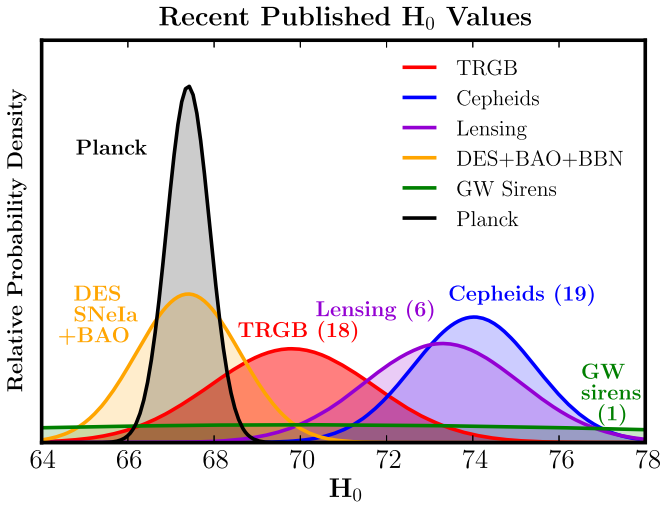

Figure 13. Relative probability density distributions for several recent determinations of H_0 (CMB: Planck Collaboration et al. 2018; DES SNeIa + BAO: Macaulay et al. 2018; TRGB: Freedman et al. 2019; Lensing: Wong et al. 2019; Cepheids: Riess et al. 2019; gravitational wave sirens: Abbott et al. 2017).

self-consistently being determined by and for the TRGB stars themselves. Our (combined) value of $A_I = 0.165 \pm 0.02$ mag lies within one sigma of the mean for other recent estimates of the LMC extinction. It differs by 0.005 mag from that adopted in Freedman et al. (2019).

Adopting the *HST*/ACS calibration from Freedman et al. (2019), applied to a sample of nearby galaxies with TRGB distances, and tied to the Carnegie Supernova Project distant sample of SNe Ia, we determine a value of $H_0 = 69.6 \pm 0.8$ ($\pm 1.1\%$ stat) $\pm$ 1.7 ($\pm 2.4\%$ sys) km s^{-1} Mpc^{-1}.

We note that the measurement of the extinction can continue to be improved with future study. We have already obtained new high-resolution optical data using the 6.5 m Magellan Baade telescope for several nearby galaxies, in order to further improve the accuracy of our LMC reddening estimate.

Results published recently by Y19 differ from ours for several reasons. The first point of divergence is that we use the OGLE-III photometry of the SMC to derive the LMC extinction, rather than attempting, as Y19 do, to correct the problematic photometry of Zaritsky et al. (2002). Second, Y19 adjust the Freedman et al. (2019) result for single-band extinction alone, neglecting the concomitant, iterative corrections for reddening, which must be applied (as discussed in detail in Section 3.2). Third, Y19 apply a theoretical correction for metallicity effects to the Freedman et al. (2019) result for the IC 1613 calibration, neglecting the fact that the method outlined in Freedman et al., and again in more detail in this paper, already explicitly accounts for metallicity. The methodology employed in Y19 differs significantly from the analysis process that we have explicated here and applied in Freedman et al., and in major respects their interpretation of the method is simply in error. We conclude that our direct measurement of the LMC TRGB extinction *based on the TRGB stars themselves* is to be preferred over an arbitrary value determined for a different population of stars, and which is systematically low compared to other recent studies in the published literature (see Figure 8). Despite these differences, we note that the Freedman et al. (2019) and Y19 H_o values agree to within 1σ.

An accurate measure of the extinction to TRGB stars in the LMC will remain an important (but not the only) component of the calibration and application of the TRGB method to the determination of H_o. Future improvements will come from higher-precision, multi-wavelength photometry for LMC TRGB stars, and from new multi-wavelength photometry and *Gaia* DR3 parallaxes to their counterparts in the halo of the Milky Way. Future *Gaia* parallaxes for Milky Way globular clusters will also strengthen the Galactic calibration of the TRGB. We note that the TRGB method, as applied to the determination of H_0, is relatively new compared to the application of the Cepheid distance scale or cosmic microwave background measurements. Additional calibrators for the TRGB method will be forthcoming from *HST* and eventually with the *James Webb Space Telescope*. The high precision measured for the TRGB, and the ability to work in the isolated, low-reddening halos of galaxies of all morphological types, will be critical for breaking the impasse in current measurements of H_0.

We thank Andre Udalski and collaborators for making their Magellanic Cloud surveys publicly available. We thank Lars Bildsten for several enlightening discussions on the TRGB at a number of recent meetings. Early comments and suggestions from Adam Riess, regarding the optical calibration of the LMC stars, are gratefully acknowledged. We also thank the Padova Group, and especially Leo Giradi, for making their stellar evolution code, PARSEC, publicly and easily available for use on the web. We thank the Observatories of the Carnegie Institution for Science and the University of Chicago for their support of our long-term research into the calibration and determination of the expansion rate of the universe. Support for this work was provided in part by NASA through grant number HST-GO-13691.003-A from the it Space Telescope Science Institute, which is operated by AURA, Inc., under NASA contract NAS 5-26555. M.G.L. is supported by a grant from the National Research Foundation (NRF) of Korea, funded by the Korean Government (NRF-2019R1A2C2084019). Partial support for this work was provided by NASA through Hubble Fellowship grant #51386.01 to R.L.B. by the Space Telescope Science Institute, which is operated by the Association of Universities for Research in Astronomy, Inc., for NASA, under contract NAS 5-26555. This publication made use of data products from the Two Micron All Sky Survey, which is a joint project of the University of Massachusetts and the Infrared Processing and Analysis Center/California Institute of

Technology, funded by the National Aeronautics and Space Administration and the National Science Foundation. We also made use of the NASA/IPAC Extragalactic Database (NED) which is operated by the Jet Propulsion Laboratory, California Institute of Technology, under contract with the National Aeronautics and Space Administration. And, finally, we thank the referee for many constructive suggestions and points of clarification that helped to improve this paper.

Appendix
Comments on the Yuan et al. (2019) Paper

After reverse-engineering the calibration plot presented in Freedman et al. (2019), Y19 concluded that the results of our paper were incorrect. Here, we show that there are a number of misunderstandings and incorrect assumptions made by Y19. For example, in their critique of our results based on a differential analysis of the LMC reddening with respect to the SMC and IC 1613, they (back)-apply corrections to the Freedman et al. (2019) result, leading them to erroneous conclusions. We now list and discuss these issues in detail below.

1. *The SMC: use of the Zaritsky* et al. *(2002) data.* Y19 noted that the OGLE-III photometry for the SMC is less subject to blending issues than that available to Freedman et al. (2019), which was based on the survey of Zaritsky et al. (2002; hereafter Z02). As seen in Section 3.2, we have now analyzed the OGLE-III photometry, and emphasize that the Y19 criticism of the SMC reddening (as being due to blending issues) is no longer applicable to the results in this current paper. Indeed, as shown in their Figure 5, there is no apparent trend of the photometric offsets with local number density. We note that the difference in reddening, resulting from adopting the OGLE-III data over the Z02 data for the SMC, amounts to only +0.005 mag, and falls within the one-sigma uncertainty quoted by Freedman et al. (2019).
2. *Y19 "correction" to the Z02 SMC data*. We note that the re-analysis by Y19 for the SMC data is based on the Z02 photometry, which they have demonstrated are less accurate. Rather than use the better OGLE-III photometry, Y19 correct the Z02 results for blending effects, and then back-correct the Freedman et al. (2019) results. We point out that in doing this "back-correction," Y19 correct for a magnitude effect (the extinction), but do not iteratively and simultaneously correct for the color (reddening) term that must also be accounted for (see the discussion in Section 3.2 and Figures 3, and 4; without taking these effects into account, the extinction and reddening terms will be underestimated.) We further note their blending correction may or may not be applicable to the actual stars used in the Freedman et al. analysis. We conclude that the Y19 "back-corrected" result for the SMC extinction value based on the Z02 data is incorrect.
3. *IC 1613: Y19 statement about the "V" data*. Y19 conclude that they cannot make use of the data for IC 1613, used here and in Freedman et al. (2019), for a photometry comparison. They state that "the IC 1613 detections are presented in Hatt et al. (2017) where ground-based V photometry is calibrated to a redder ACS filter, F606W." We wish to be clear here that, as outlined in Section 3.2, we do not make use of such a transformation for our derived fit to the extinction law. The optical data that enter into the derivation of the extinction fit are zeroed to the *VI* photometry from Hatt et al. (2017), based on the well-calibrated set of Stetson photometry (http://www.cadc-ccda.hia-iha.nrc-cnrc.gc.ca/en/community/STETSON/standards/). In Freedman et al. and Hatt et al. we compare these ground-based data to the F814W data for IC 1613, and find agreement to ±0.02 mag (1%). To briefly summarize, we fit an extinction law to a multi-wavelength (*VIJHK*) set of data to determine A_I for the LMC, which we then apply to the *I*-band TRGB magnitude. The transformation to the *HST*/ACS F814W system is done only in the last step, when we calibrate the TRGB magnitude. The data referred to in Hatt et al. are not used and are not relevant for the analysis for determining the reddening described here.
4. *IC 1613: Y19 double correction for metallicity*. Y19 cite McQuinn et al. (2019), stating that "the use of a single slope to rectify" the TRGB for its color dependence at different metallicities produces differences in the TRGB of ∼0.04 mag for the difference in metallicity between −2 and −1 dex. Quoting directly, Y19 state that they "naively use the comparison in McQuinn et al. (2019) for the same SFH and Δ[Fe/H] (from −2 to −1 dex)" to illustrate the impact of rectifying the TRGB colors on the extinction estimate. These corrections amount to 0.026, 0.033 and 0.038 mag, making the TRGB stars fainter in *J*, *H* and *K*, respectively, and amounting to −0.019 and −0.014 mag offsets in *V* and *I*, respectively, making stars at those wavelengths brighter. After making these corrections, Y19 find a value for $A_I^{\rm LMC} = 0.10$ mag "in agreement with earlier determinations." We have discussed the (broad) range of earlier published reddening determinations in Section 3.5. However, we point out that the correction applied by Y19 for metallicity is simply incorrect, as illustrated by both the theoretical isochrones shown in Figures 1 and 2, and by the empirical CMDs shown in Figures 5 and 6. The well-known metallicity-tracking trends with color for RGB stars are *directly* exhibited in the CMDs. Y19 have thus apparently effectively added corrections for metallicity effects twice.

   We summarize the results of Figure 2 once again here. The TRGB stars at *I*, for example, map uniquely into their respective positions in the CMDs at other colors, and they do so in accordance with their metallicities as reflected and calibrated by their colors. As expected, the most metal-rich stars are fainter at *V*, and brighter at *K*. These other wavebands do not have a flat distribution with magnitude; there is a well-defined *run* or sequence of magnitude with color *that is not arbitrary*. Using a self-consistent sample of *precisely the same RGB stars* defined in the *I*-band CMD, one can make use of the (very fortunate) fact that the optical (*V* and *I*), and the near-infared (*JHK*) bandpasses exhibit distinctly different behaviors with metallicity. The opposite signs of the optical/near-infrared behavior resulting from metallicity differences are in contrast to that of extinction, which is a steadily decreasing function of inverse wavelength. The different dependences

of metallicity and extinction with wavelength thus allows the two effects to be separated, and the extinction can be independently measured, as demonstrated in Figure 3, and detailed in Section 3.1.

5. *LMC reddening*. Y19 argue that the extinction estimates from Haschke et al. (2011) are the best available estimate of the LMC reddening. The recent results of Gorski et al. (2020) dispute that claim, arguing for reddenings that are 0.06 mag higher in $E(B-V)$ than the Haschke et al. calibration, which is based on red clump stars and RR Lyrae stars. Unlike the case for TRGB stars, the evolutionary tracks for red clump stars are well known to be strong functions of both age and metallicity (see, for example, Girardi & Salaris 2001; Williams et al. 2009). Finally, as discussed by Joshi & Panchal (2019), and in agreement with Gorski et al., it is found that the Haschke extinction estimates are systematically lower than all other estimates reviewed in their summary. For completeness, we note also that a higher value for the red clump star extinction is also found in the earlier analysis by Pawlak (2016). At the time of their study, Jang & Lee (2017a) had no direct estimate of the TRGB extinction and adopted the Haschke et al. extinction value, with its originally published uncertainty of 0.07 mag.

ORCID iDs

Wendy L. Freedman https://orcid.org/0000-0003-3431-9135
Barry F. Madore https://orcid.org/0000-0002-1576-1676
Taylor Hoyt https://orcid.org/0000-0001-9664-0560
In Sung Jang https://orcid.org/0000-0002-2502-0070
Rachael Beaton https://orcid.org/0000-0002-1691-8217
Myung Gyoon Lee https://orcid.org/0000-0003-2713-6744
Jill Neeley https://orcid.org/0000-0002-8894-836X
Jeffrey Rich https://orcid.org/0000-0002-5807-5078

References

Abbott, B. P., Abbott, R., & Abbott, T. D. 2017, Natur, 551, 85
Arenou, F., Luri, X., Babusiaux, C., et al. 2018, A&A, 616, 17
Bellazzini, M. 2008, MmSAI, 79, 440
Bellazzini, M., Ferraro, F. R., & Pancino, E. 2001, ApJ, 556, 635
Bildsten, L., Paxton, B., Moore, K., et al. 2012, ApJL, 744, 6
Bressan, A., Marigo, P., Girardi, L., et al. 2012, MNRAS, 427, 127
Chen, S., Richer, H., Caiazzo, I., & Heyl, J. 2018, ApJ, 867, 132
Cutri, R. M., Skrutskie, M. F., van Dyk, S., et al. 2006, Explanatory Supplement to the 2MASS All Sky Data Release and Extended Mission Products, https://irsa.ipac.caltech.edu/data/2MASS/docs/releases/allsky/doc/explsup.html
da Costa, G. S., & Armandroff, T. E. 1990, AJ, 100, 162, (DCA90)
Dalcanton, J. J., Williams, B. F., Melbourne, J. L., et al. 2012, ApJS, 198, 6
Dalcanton, J. J., Williams, B. F., Seth, A. C., et al. 2009, ApJS, 183, 67
Fitzpatrick, E. 1999, PASP, 111, 63
Freedman, W. L. 1988, ApJ, 326, 691
Freedman, W. L., Madore, B. F., Hatt, D., et al. 2019, ApJ, 882, 34
Freedman, W. L., Wilson, C. D., & Madore, B. F. 1991, ApJ, 372, 455
Girardi, L., & Salaris, M. 2001, MNRAS, 323, 109
Gorski, M., Zgirski, B., Pietrzynski, G., et al. 2020, arXiv:2001.08242
Graczyk, D., Pietrzyński, G., Thompson, I. B., et al. 2014, ApJ, 780, 59
Harris, W. E. 1996, AJ, 112, 1487
Haschke, R., Grebel, E. K., & Duffau, S. 2011, AJ, 141, 158
Hatt, D., Beaton, R. L., Freedman, W. L., et al. 2017, ApJ, 845, 146
Hoffmann, S. L., & Macri, L. M. 2015, AJ, 149, 183
Jacyszyn-Dobrzeniecka, A. M., Skowron, D. M., Mróz, P., et al. 2016, AcA, 66, 149
Jang, I.-S., & Lee, M. G. 2017a, ApJ, 835, 28
Jang, I.-S., & Lee, M. G. 2017b, ApJ, 836, 74
Joshi, Y. C., & Panchal, A. 2019, A&A, 628, A51
Karachentsev, I. D., Makarov, D. I., Sharina, M. E., et al. 2003, A&A, 398, 479
Lee, M. G., Freedman, W. L., & Madore, B. F. 1993, ApJ, 417, 553
Macaulay, E., Nichol, R. C., Bacon, D., et al. 2018, arXiv:1811.02376v2
Madore, B. F., Freedman, W. L., Hatt, D., et al. 2018, ApJ, 858, 11
Mager, V., Madore, B. F., Freedman, W. L., et al. 2008, ApJ, 689, 721, (Mag08)
Makarov, D., Makarova, L., Rizzi, L., et al. 2006, AJ, 132, 2729
Marigo, P., Girardi, L., Bressan, A., et al. 2017, ApJ, 835, 77
McQuinn, K. B. W., Boyer, M., Skillman, E. D., et al. 2019, ApJ, 880, 63
Mould, J., & Sakai, S. 2008, ApJL, 686, 75
Mould, J., & Sakai, S. 2009, ApJ, 697, 996
Mould, J. R., Clementini, G., & Da Costa, G. 2019, PASA, 36, 1
Paczyński, B. 1997, in Proc. StSci Symp., Extragalactic Distance Scale, ed. M. Livio, M. Donahue, & N. Panagia (Cambridge: Cambridge Univ. Press), 273
Pawlak, M. 2016, MNRAS, 547, 4323
Pietrzyński, G., Graczyk, D., Gallenne, A., et al. 2019, Natur, 567, 200
Planck Collaboration, Aghanim, N., Akrami, Y., et al. 2018, arXiv:1807.06209
Riess, A. G., Casertano, S., Yuan, W., et al. 2019, ApJ, 876, 85
Rizzi, L., Tully, R. B., Makarov, D., et al. 2007, ApJ, 661, 815
Sakai, S., Ferrarese, L., Kennicutt, R. C., Jr., & Saha, A. 2004, ApJ, 608, 42
Salaris, M., & Cassisi, S. 1997, MNRAS, 289, 406
Schlafly, E. F., & Finkbeiner, D. P. 2011, ApJ, 737, 103
Schlegel, D. J., Finkbeiner, D. P., & Davis, M. C. 1998, ApJ, 500, 525
Scowcroft, V., Freedman, W. L., Madore, B. F., et al. 2013, ApJ, 773, 106
Serenelli, A., Weiss, A., Cassisi, S., et al. 2017, A&A, 606, 33
Thompson, I. B., Udalski, A., Dotter, A., et al. 2020, MNRAS, 492, 4254
Udalski, A., Szymanski, M. K., Soszynski, I., et al. 2008, AcA, 58, 69
Ulaczyk, K., Symanski, M. K., Udalski, A., et al. 2012, AcA, 62, 247
Valenti, E., Ferraro, F. R., & Origlia, L. 2004a, MNRAS, 351, 1204
Valenti, E., Ferraro, F. R., & Origlia, L. 2004b, MNRAS, 354, 815
Williams, B. F., Dalcanton, J. J., Seth, A. C., et al. 2009, AJ, 137, 419
Wong, K. C., Suyu, S. H., Chen, G. C.-F., et al. 2019, arXiv:1907.04869
Yuan, W., Riess, A. G., Macri, L. M., et al. 2019, ApJ, 886, 61, (Y19)
Zaritsky, D., Harris, J., Thompson, I., et al. 2002, AJ, 123, 855
Zaritsky, D., Harris, J., Thompson, I., et al. 2004, AJ, 128, 1606